

QUANTIFYING UNCERTAINTY IN LASER POWDER BED FUSION ADDITIVE MANUFACTURING MODELS AND SIMULATIONS

Tesfaye Moges¹, Wentao Yan¹, Stephen Lin², Gaurav Ameta¹, Jason Fox¹, and Paul Witherell¹

¹National Institute of Standards and Technology, Gaithersburg, MD 20899

²Northwestern University, Evanston, IL 60208

Abstract

Various sources of uncertainty that can potentially cause variability in the product quality exist at different stages of the laser powder bed fusion (L-PBF) process. To implement computational models and simulations for quality control and process optimization, quantitative representation of their predictive accuracy is required. In this study, a methodology to estimate uncertainties in L-PBF models and simulations is presented. The sources of uncertainty, including those due to modeling assumptions, numerical approximation, input parameters, and measurement error, are discussed in detail and quantified for low and high-fidelity melt pool simulation models. A design of experiments (DOE) approach is leveraged to quantify uncertainty due to input parameters and investigate their effects on output quantities of interest (QoIs). The result of this work is essential for understanding the tradeoffs in model fidelity and guiding the selection of a model suitable for its intended purpose.

Keywords: Additive manufacturing, Powder bed fusion, Uncertainty quantification, Melt pool model, Design of experiments

Introduction

Metal additive manufacturing (AM) builds metallic parts layer upon layer directly from a 3D model. Due to its capability of producing metallic components having complex geometry and internal structures, it has become popular in different sectors, such as aerospace and automotive (scaffold cooling and weight reduction) and biomedical implants (prosthesis and femur structures) [1–3]. Laser powder bed fusion (L-PBF) is the most widely used metal AM process. In L-PBF, a thin layer of powder material is selectively scanned using a laser as the energy source to fuse powder particles together. In this process, powder layer formation and laser scanning operations are repeated multiple times until the final part is produced [4]. Due to the inherent nature of the L-PBF process, multiple physical phenomena and process parameters are involved at different stages. The process is governed by a variety of physical mechanisms, such as powder layer formation, laser-powder particle interaction, heat transfer, fluid dynamics of the melt pool, phase transformations, and microstructure evolution. Any variation encountered in these mechanisms potentially affects the quality of the final part. A major barrier that hinders full adoption of the L-PBF technology is inconsistent product quality.

To improve the quality of the product, it is important to investigate the sources of variability, quantify the uncertainties that occur at different stages of the process, and determine the magnitude of their effects on output quantities of interest. To quantify the uncertainties and analyze the sensitivity of input parameters, extensive research efforts have been continued based on physical experiments and computational models and simulations. Since performing uncertainty quantification in the L-PBF process using physical experiments is often expensive, computational models and simulations are promising tools to understand the dynamics, complex phenomena, and variabilities existing in the process. Although promising, computational models and simulations have not been fully utilized in quality control and process optimization due to lack of quantitative representation of their predictive accuracy. Without knowledge of the degree of accuracy of the L-PBF models and simulations, it is challenging to select a suitable model for the intended purpose. Therefore, it is necessary to identify and quantify the potential sources of uncertainty to investigate the predictive accuracy of such models and simulations.

This paper presents the sources of uncertainty in computational models and in the experimental validation and a methodology to quantify the uncertainties that exist in the L-PBF models. The predictive accuracy of such models strongly depends on the included and neglected physics of the process. *Modeling uncertainty* originates from the modeling assumptions that neglect part of the physical phenomena of a process. In addition, computational models require several input parameters including process parameters and material properties to represent the physical scenario of the process. However, the value of some parameters cannot always be known precisely and may exhibit inherent temporal fluctuations. Therefore, there is an associated *parameter uncertainty* in the computational models due to unknown input parameters. Moreover, the mathematical equations used to formulate the physical phenomena are difficult to be solved analytically, and various numerical methods have been used to discretize the system into finite elements and temporal transient phenomena into time steps to obtain an approximate solution. This discretization introduces *numerical uncertainty* in the computational models. Lastly, to validate the simulation results against measurement data, experimental results introduce *measurement uncertainty* due to imprecise measurement methods. In this study, all of these sources of uncertainty are quantified for the Rosenthal's semi-analytical thermal model [5,6]. In addition, we recommend best practices for quantifying model uncertainty for a finite element method (FEM)-based thermal model [7].

In this paper, we first briefly present the state-of-the-art in uncertainty quantification for L-PBF models. We then explore the shortcomings of previous work by classifying and characterizing sources of uncertainty in L-PBF models. Then, we examine, model, and evaluate all uncertainty sources of a L-PBF model using a case study through a standards-based approach. We view this work to be an essential step to report on requirements for further standardization and ultimately guide the selection of models suitable for their intended purpose.

Background

Since experimental-based part qualification for the L-PBF process is time consuming and costly, model-based qualification has been the focus of much research in the AM community. Several computational models have been developed to simulate the physical mechanisms and predict output quantities of interest at different stages of the process [8,9]. These models can be classified as powder bed models [10,11], heat source models [12,13], melt pool models [14,15], solidification models [16,17], and residual stress and distortion models [18,19]. Though computational models are different in their formulation, they share similar abstraction and characteristics [20,21]. The fidelity of the L-PBF models can be evaluated by identifying the various sources of uncertainty and quantifying their individual contribution to the overall prediction uncertainty [20].

Uncertainty quantification (UQ) of AM processes has recently been receiving increasing attention and some research efforts exist based on physical experiments, modeling and simulations [9,22,23]. Several reports have focused on experimentally investigating the effects of process parameters and material properties on the output quantities of interest and performing uncertainty quantification and sensitivity analysis [24–27]. Since AM processes possess a large number of parameters that influence the quality of a product, experimental-based UQ is expensive [28]. Thus, model-based UQ is getting attention for part qualification. Moser et al. [29] used a stochastic collocation approach to identify the most important parameters that affect the fidelity of FEM thermal model. Assuming probability distribution functions (PDFs) of input parameters, such as powder density, thermal conductivity, specific heat, particle diameter, and simulation time, the PDF of peak temperature is predicted. Ma et al. [30] used fractional factorial DOE to identify the critical process parameters and material properties that significantly influence peak temperature in FEM-based thermal model. Nath et al. [31] conducted uncertainty analysis on a FEM-based melt pool model that determined temperature profile and investigated uncertainty propagation to the solidification model to quantify the uncertainty in the grain size distribution of the microstructure. There have also been research efforts on implementing UQ methods for powder-scale AM model by developing surrogate models [32].

Previous studies have mainly focused on investigating the effects of input parameters on output quantities of interest and only quantifying parameter uncertainty. However, computational models exhibit all of the abovementioned sources of uncertainty and UQ-based study should include the remaining uncertainty sources to accurately determine the fidelity of a model. Recently, Lopez et al. [5] identified the four sources of uncertainty and conceptualized the quantification approach on the Isotherm Migration Method (IMM) model [6] by choosing melt pool width as the output quantity of interest. We further extend UQ approaches in the present study to quantify *all* sources of uncertainty and analyze their contribution towards model fidelity considering semi-analytical and FEM-based L-PBF melt pool models as a case study.

Uncertainty Quantification of Computational Models

In this section, we present a detailed discussion of the sources of uncertainty and their quantification, including those due to modeling assumptions, numerical approximation, input parameters, and measurement error of L-PBF process models.

Modeling Uncertainty

Computational models do not exactly represent the physical mechanisms that exists in L-PBF process as they are developed based on assumptions that neglect or simplify some phenomena. Thus, there is always a discrepancy between simulation results and true physical mechanisms. Modeling uncertainty originates from assumptions and simplifications made in computational models. There are a number of predictive models in the literature to represent the same L-PBF physical process [8,9]. These models are developed based on different assumptions and, therefore, there may be a significant discrepancy in their predictive accuracy due to modeling uncertainty. For example, to determine the packing density of the powder bed, powder bed models have been developed based on the Raindrop algorithm or the discrete element method. These models can induce different results and have different fidelity due to the different assumptions considered including those for powder particles shape, size and distribution, inter-particles forces, and boundary conditions. Similarly, there are various melt pool models in the literature to determine the temperature field and melt pool dimensions in the L-PBF process. These models are developed based on Rosenthal's semi-analytical thermal model, on a FEM thermal model, on a lattice Boltzmann approach, or on computational fluid dynamics (CFD). These models have different assumptions in terms of considering powder bed as a continuum or as particles, energy source as a point or distributed, and absorbed energy as a surface or volumetric distribution. There are also differences in considering other physical phenomena, such as surface tension, the Marangoni effect, recoil pressure, vaporization, capillary, and wetting. Although these models are developed for predicting the same output quantities of interest, their modeling uncertainty results in different predictive accuracy due to the different assumptions they considered. Therefore, it is important to quantify modeling uncertainty of computational models to determine their degree of predictive accuracy.

To quantify modeling uncertainty, simulation results S of the predictive model need to be validated against the experimental data D . The ASME V&V-20 standard [33], which discusses the sources of uncertainty and UQ methods in heat transfer and fluid mechanics models, can be suitable for L-PBF models as it involves thermally-activated consolidation processes [5]. The interval within which modeling error falls is characterized by $\delta_{model} \in [E \pm u_{val}]$ where, E is the comparison error between simulation result S and measurement data D , and u_{val} is validation uncertainty that accounts for all sources of uncertainty. Assuming that they are independent, it can be computed as:

$$u_{val} = \sqrt{u_{num}^2 + u_{input}^2 + u_D^2}, \dots\dots\dots(1)$$

where u_{num} , u_{input} , and u_D are numerical uncertainty, parameter uncertainty, and measurement uncertainty, respectively. The following sub-sections discuss the uncertainty sources and quantification methods of these uncertainties.

Numerical Uncertainty

Due to the complexity of the L-PBF process, constitutive equations that approximate the physical phenomena are not often solved using analytical methods. Numerical methods that discretize the time and length variables are used to solve the partial differential equations. For the L-PBF process, predictive models are commonly developed based on numerical methods, such as finite element models, discrete element models, lattice Boltzmann method, and computational fluid dynamics studies. Thus, the choice of finite time and length resolution introduces numerical error that undermines the accuracy of the simulation results of the output quantities of interest [34]. For example, the element size or number of elements in an FEM-based thermal model and mesh discretization to represent the change in temperature in semi-analytical thermal model cause numerical uncertainty in the predicted melt pool width. Since most of predictive models are computationally expensive, reduced order and surrogate models are used to statistically represent the simulation models. This can introduce additional uncertainty due to the limited number of training data used to build the representative model.

Numerical uncertainty can be quantified using a grid convergence index (GCI) developed by Roache [35]. The GCI is an error percentage that provides an estimate of the coverage interval within which the numerical error will likely lie. Numerical uncertainty is the GCI percentage of the value of the output quantity of interest. The GCI is obtained by multiplying the absolute value of Richardson extrapolation error by a safety factor determined through empirical studies and given by:

$$GCI = F_s \frac{\epsilon_{ext}}{r_{21}^p - 1}, \dots\dots\dots(2)$$

$$\epsilon_{ext} = \left| \frac{f_{ext}^{21} - f_1}{f_{ext}^{21}} \right|, \quad f_{ext}^{21} = \frac{r_{21}^p f_1 - f_2}{r_{21}^p - 1}, \quad p = \frac{\ln(|f_3 - f_2|/|f_2 - f_1|) + q(p)}{\ln r_{21}}, \dots\dots\dots(3)$$

where, $F_s = 1.25$ is factor of safety; f_1 , f_2 , and f_3 are three simulation results at fine h_1 , finer h_2 , and finest h_3 mesh sizes, respectively; and $r_{21} = h_2/h_1$ is the mesh refinement ratio. The order of convergence p is determined using Equation (3). For a constant mesh refinement ratio, $q(p) = 0$. Otherwise, $q(p) = \ln[(r_{21}^p - s)/(r_{32}^p - s)]$ and $s = \text{sign}[(f_3 - f_2)/(f_2 - f_1)]$, and the convergence order is solved iteratively with initial guess $q(p) = 0$.

Parameter Uncertainty

Computational models require prior determination of input parameters to represent the behavior of a process. The values of some parameters are not precisely known due to natural variation in the system or lack of sufficient data and knowledge to determine the exact value. Therefore, the assigned value has uncertainty that propagates into an output quantity of interest.

The sources of uncertainty can take one of two forms: aleatory and epistemic. Aleatory uncertainty arises due to natural variation existing in the parameters and in the performance of the system. For instance, inherent drift and fluctuation in the laser and galvanometer systems cause aleatory variability in the laser power and scan speed in L-PBF process. On the other hand, epistemic uncertainty arises as a result of lack of knowledge regarding the behavior of a system. For example, the determination of the absorption coefficient of a powder bed is not well established due to lack of a convincing measurement method and could be resolved by introducing additional information. This study considers the joint effect of aleatory and epistemic uncertainties instead of distinguishing them separately as suggested by Roache [35].

To quantify the input parameter uncertainty, first the uncertainty associated with the parameters is captured in a form of distribution, nominal value, and standard deviation. Then, the sources of uncertainty of these parameters propagate into output quantity of interest through computational models or reduced order models. In this study, a design of experiments (DOE) method is used to quantify input parameter uncertainty by formulating a reduced order formulation. Experimental design is a suitable technique to identify the most important factors that have significant impact on the response variable and develop a response surface model that approximates the original process [36]. In the present study, a fractional factorial design of experiments approach is used to plan the design matrix for simulation runs and quantify input parameter uncertainty, choosing melt pool width as a response variable. The detailed procedure and discussion on implementing DOE for UQ of input parameters is presented in the case study section.

Measurement Uncertainty

Since experimental data is required to validate the simulation results, measurement uncertainty is important in the UQ process to determine the predictive accuracy of L-PBF models. Measurement uncertainty mainly depends on the methods and equipment used for data acquisition. To understand the process-structure-properties-performance chain of the L-PBF process, measurement results during pre-process, in-process, and post-process are necessary [37]. For example, uncertainties related to measurement methods used to determine the powder packing structure that depends on metal powder characterization (such as powder size, morphology, density, and distribution [38,39]), non-intrusive infrared thermography, and pyrometry to measure surface temperature of the heat affected zone [37]. Measurement uncertainty is quantified as per the guide to the expression of uncertainty in measurement (GUM) that standardized the evaluation and expression of uncertainty in measurement [40].

Propagation of Uncertainty in L-PBF Models

Uncertainty is propagated through L-PBF models in the manner depicted in Figure 1. Input uncertainty enters each different model with input parameters. Outputs of some models are incorporated as inputs in other models. For this reason, it is required to understand the propagated effects of uncertainty through a composition of models. Besides parameter uncertainty, modeling and numerical uncertainties also propagate to outputs.

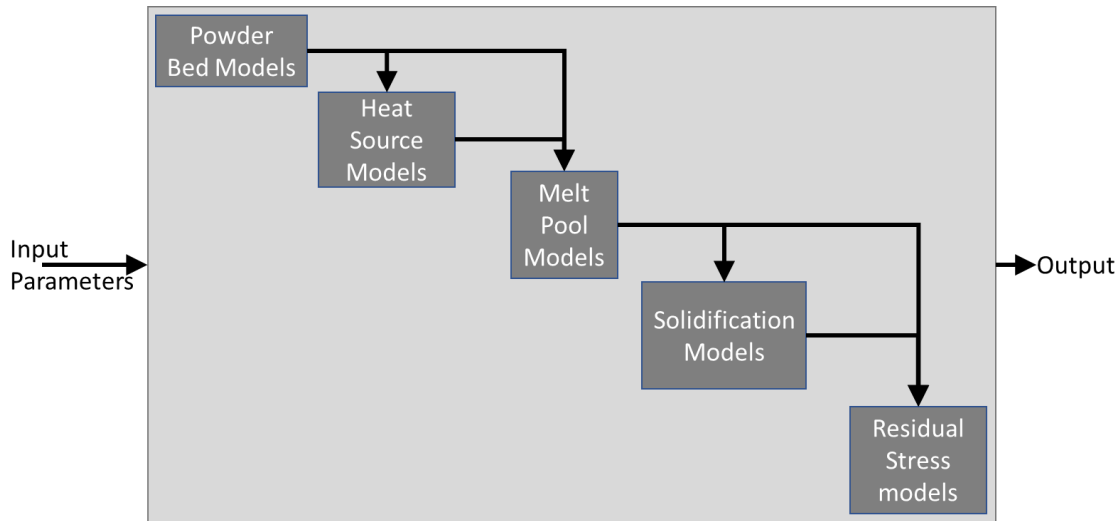


Figure 1: Flow of uncertainty in L-PBF models.

Case Study: UQ in a Semi-Analytical- and FEM-Based Melt Pool Models

In this case study, semi-analytic- and FEM-based melt pool models are selected for the purpose of quantifying all sources of uncertainty in the L-PBF process as shown in the previous section. In a semi-analytical-based melt pool model, the heat conduction equation is transformed into a set of ordinary differential equations to determine the isotherm velocities on the surface of the powder bed in terms of positions and temperature derivatives. The phase change that occurs during the process is taken into consideration to incorporate the effect of the internal energy difference between solid and liquid states at melting temperature, which is given by the latent heat of fusion of a material. The melt pool width is predicted directly from the isotherm position by assigning a melting temperature on one of the isotherms. The model is first developed for laser cladding [6] and adjusted for prediction of melt pool dimensions in L-PBF [5]. Although this model considers the temperature-dependent material properties and provides results in an efficient manner, there are a number of assumptions related to the phenomena of the process. The heat source is assumed as a point source, which is not in conjunction with reality instead of a distributed one. The melt pool flow and distribution of particles in a powder bed are also ignored. This simplification and assumptions are expected to increase modeling error. The discretization of the temperature increment to represent the isotherms creates numerical error.

The FEM-based melt pool model is the most popular method to simulate the L-PBF process [8]. It discretizes the powder bed into a finite number of elements by forming a mesh to solve the partial differential equation governing the system in order to estimate thermal field and melt pool characteristics. The main assumption of this model is that the powder bed is considered a homogenous continuum material instead of a distribution of powder particles. The physical phenomena encountered in the melt pool dynamics, such as surface tension and the Marangoni effect, are ignored, which creates modeling error. The FEM-based melt pool model used for present work is proposed by Smith et al. [7] assuming a heat source with Gaussian distribution.

Computational Design of Experiments

To make the uncertainty quantification process for a model having many parameters more computationally practical, a DOE approach, which is widely used to identify the most important parameters that have major influence on the output, is used for the present work. As the number of factors increases, investigating the effect of each of the factors along with their interactions on the output quantities of interest using full factorial DOE is infeasible due to high computational cost. Therefore, a fractional factorial DOE is chosen to sample some of the most important runs that can provide the necessary information about the main effects and second-order interactions [41].

For the semi-analytical-based melt pool model, all the input parameters (i.e. nine factors) used in the model are selected for DOE analysis. A 2_{IV}^{9-4} fractional factorial design that represents two levels for each factor and four resolution is selected. In this design, no main effects are confounded with any other main effect and two-factor interactions. We select 2_{IV}^{10-5} fractional factorial design having ten factors for the FEM-based melt pool model. These designs require $2^5 = 32$ simulation runs for each model. Normal distributions, which commonly used in UQ to represent the variations of input parameters due to random and imperfect knowledge, are assumed for the selected factors and the design matrices for the semi-analytical- and FEM-based melt pool models are outlined in Tables 1 and 2, respectively.

Table 1: DOE plan for the semi-analytical-based melt pool model

Factor	X1	X2	X3	X4	X5	X6	X7	X8	X9
Name	Laser power	Scan speed	Preheat temperature	Density	Specific heat capacity	Thermal conductivity	Absorption coefficient	Latent heat of fusion	Melting temperature
Symbol	P	v	T_o	ρ	c_p	k	A	h_l	T_m
Nominal value	195	0.8	293	$\rho(T)$	$c_p(T)$	$k(T)$	0.4	2.97×10^5	1593
Unit	W	m/s	K	kg/m^3	J/kgK	W/mK		J/kg	K
Std. dev.	2.5%	1.5%	1%	1%	3%	3%	25%	5%	5%
Run 01	-	-	-	-	-	+	+	+	+
Run 02	+	-	-	-	-	+	-	-	-
Run 03	-	+	-	-	-	-	+	-	-
Run 04	+	+	-	-	-	-	-	+	+
Run 05	-	-	+	-	-	-	-	+	-
Run 06	+	-	+	-	-	-	+	-	+
Run 07	-	+	+	-	-	+	-	-	+
Run 08	+	+	+	-	-	+	+	+	-
Run 09	-	-	-	+	-	-	-	-	+
Run 10	+	-	-	+	-	-	+	+	-
Run 11	-	+	-	+	-	+	-	+	-
Run 12	+	+	-	+	-	+	+	-	+
Run 13	-	-	+	+	-	+	+	-	-
Run 14	+	-	+	+	-	+	-	+	+
Run 15	-	+	+	+	-	-	+	+	+
Run 16	+	+	+	+	-	-	-	-	-
Run 17	-	-	-	-	+	-	-	-	-
Run 18	+	-	-	-	+	-	+	+	+
Run 19	-	+	-	-	+	+	-	+	+
Run 20	+	+	-	-	+	+	+	-	-
Run 21	-	-	+	-	+	+	+	-	+
Run 22	+	-	+	-	+	+	-	+	-
Run 23	-	+	+	-	+	-	+	+	-
Run 24	+	+	+	-	+	-	-	-	+
Run 25	-	-	-	+	+	+	+	+	-
Run 26	+	-	-	+	+	+	-	-	+
Run 27	-	+	-	+	+	-	+	-	+
Run 28	+	+	-	+	+	-	-	+	-
Run 29	-	-	+	+	+	-	-	+	+
Run 30	+	-	+	+	+	-	+	-	-
Run 31	-	+	+	+	+	+	-	-	-
Run 32	+	+	+	+	+	+	+	+	+

The design matrices in Tables 1 and 2 are coded as (-) and (+) to represent the low (nominal value minus standard deviation) and high (nominal value plus standard deviation) values of the two levels for each of the factors and defines the 32 simulation runs. The matrices in Tables 1 and 2 are arranged in such a way that all columns are orthogonal to each other and the main and interaction effects can be independently estimated. Since the variation of input parameters and some of their values are not yet explicitly determined, the nominal values and their variations are chosen based on prior research and expert opinions [30].

Table 2: DOE plan for the FEM-based melt pool model

Factor	X1	X2	X3	X4	X5	X6	X7	X8	X9	X10
Variable name	Laser power	Scan speed	Layer thickness	Laser beam radius	Density	Specific heat capacity	Thermal conductivity	Absorption coefficient	Latent heat of fusion	Emis-sivity
Symbol	P	v	l_t	r_{beam}	ρ	c_p	k	A	h_l	ϵ
Nominal value	195	0.8	40	45	$\rho(T)$	$c_p(T)$	$k(T)$	0.4	2.97×10^5	0.4
Units	W	m/s	μm	μm	kg/m^3	J/kgK	W/mK		J/kg	
Std. dev.	2.5%	1.5%	25%	10%	1%	3%	3%	25%	5%	10%
Run 01	-	-	-	-	-	+	+	+	+	+
Run 02	+	-	-	-	-	-	-	-	-	+
Run 03	-	+	-	-	-	-	-	-	+	-
Run 04	+	+	-	-	-	+	+	+	-	-
Run 05	-	-	+	-	-	-	-	+	-	-
Run 06	+	-	+	-	-	+	+	-	+	-
Run 07	-	+	+	-	-	+	+	-	-	+
Run 08	+	+	+	-	-	-	-	+	+	+
Run 09	-	-	-	+	-	-	+	-	-	-
Run 10	+	-	-	+	-	+	-	+	+	-
Run 11	-	+	-	+	-	+	-	+	-	+
Run 12	+	+	-	+	-	-	+	-	+	+
Run 13	-	-	+	+	-	+	-	-	+	+
Run 14	+	-	+	+	-	-	+	+	-	+
Run 15	-	+	+	+	-	-	+	+	+	-
Run 16	+	+	+	+	-	+	-	-	-	-
Run 17	-	-	-	-	+	+	-	-	-	-
Run 18	+	-	-	-	+	-	+	+	+	-
Run 19	-	+	-	-	+	-	+	+	-	+
Run 20	+	+	-	-	+	+	-	-	+	+
Run 21	-	-	+	-	+	-	+	-	+	+
Run 22	+	-	+	-	+	+	-	+	-	+
Run 23	-	+	+	-	+	+	-	+	+	-
Run 24	+	+	+	-	+	-	+	-	-	-
Run 25	-	-	-	+	+	-	-	+	+	+
Run 26	+	-	-	+	+	+	+	-	-	+
Run 27	-	+	-	+	+	+	+	-	+	-
Run 28	+	+	-	+	+	-	-	+	-	-
Run 29	-	-	+	+	+	+	+	+	-	-
Run 30	+	-	+	+	+	-	-	-	+	-
Run 31	-	+	+	+	+	-	-	-	-	+
Run 32	+	+	+	+	+	+	+	+	+	+

Results and Discussion

To identify the input parameters that significantly influence the melt pool width, the main and interaction effects are computed. An effect is the amount of change in melt pool width when only the parameter under consideration is changed from its low (-) to high (+) level. A normal probability plot of the effects is used to isolate statistically significant effects of factors and their interactions from those effects that come solely from random variables. The normal probability plot is used for assessing whether or not a data set is approximately normally distributed and identifying statistically significant factors [42]. The normal probability plot of the effects for the semi-analytical-based melt pool model is shown in Figure 2. The main and interaction effects that represent x-axis in Figure 2 are calculated by subtracting the average of the response at the low level from the high level for the parameter under consideration.

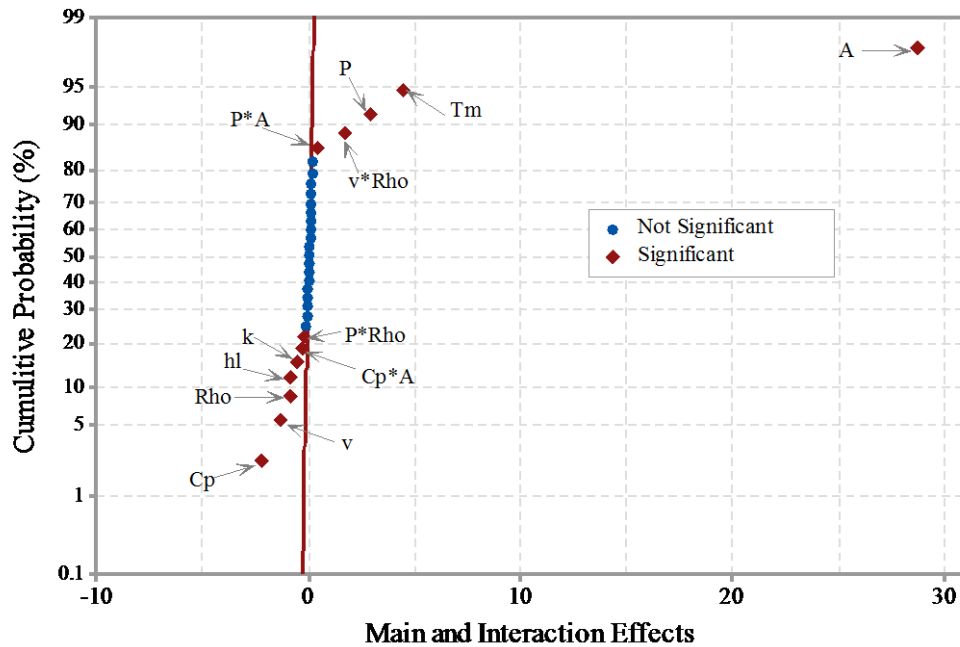


Figure 2: Normal probability plot of the semi-analytical-based melt pool model

It can be seen from normal probability plot that the main factors and some of their interactions significantly affect the melt pool width. A statistically-driven mathematical model is formulated from the DOE analysis using the identified main factors and interactions that have significant effect on the response [36]. At the given set of parameters, the mathematical model closely approximates the physics-based model. To quantify the input parameters uncertainty, a Monte Carlo approximation is conducted for 50,000 samples which are quite sufficient to get stable results and the probability distribution of the predicted melt pool width is shown in Figure 3. The average and standard deviation of the predicted melt pool width are found to be $94.2\mu\text{m}$ and $55.1\mu\text{m}$, respectively.

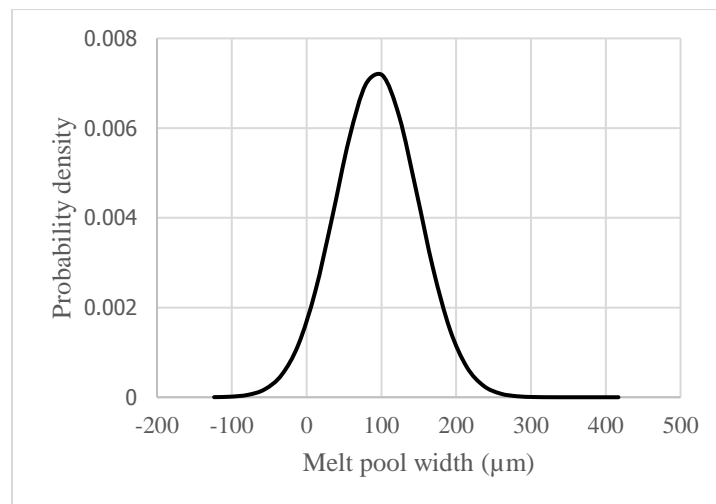


Figure 3: Normal distribution of predicted melt pool width of the semi-analytical model

The FEM-based melt pool model, though more accurate, posed difficulty when managing uncertainty with the calibration parameters. Using the set of input parameters in Table 2 the parameters that significantly affect melt pool width cannot be identified from the main and interaction effects due to the large percentage variation assumed for layer thickness and absorption coefficient. Thus, the uncertainty of the input parameters in which the model performs reasonably needed to be reconsidered.

To quantify numerical uncertainty in the semi-analytical melt pool model, simulations with a different number of isotherms having different temperature increments were run. In this case, all the input parameters are set to their nominal values. Then, the grid convergence index (GCI), which is an estimate of 95% uncertainty, was computed using Equation (2). Using the given nominal values, the estimated melt pool width in the semi-analytical model is $100.9 \pm 3.43\mu\text{m}$. Similarly, a convergence study was performed for the FEM-based melt pool model by running the simulation with different element sizes. Using the given nominal values, the estimated melt pool width for the FEM-based model is $141.0 \pm 4.23\mu\text{m}$.

To complete UQ in L-PBF models, measurement uncertainty that comes from the experiments used for validation is required. The melt pool width was measured from the image of a 1mm long scan track of IN625 captured using an optical microscope by manually tracing the edges of the track and determining the distance between the traces. The average and standard deviation of the melt pool width at 195W and 800mm/s are measured to be $132.2\mu\text{m}$ and $14.1\mu\text{m}$, and the 95% suggested confidence interval is $\pm 28.2\mu\text{m}$. In addition to this uncertainty, manually tracing the edges of the scan track causes uncertainty due to human error estimated to be $\pm 2\mu\text{m}$. This is based on the ability to determine the edge of the track accurately accounting for the focus of the image at the edge of the track and the size of pixels. More details about the experimental results and measurement methodology is given by Fox et al. [43].

The comparison of the predicted and measured melt pool width by the two models at a given laser power and scan speed combination is shown in Figure 4. Assuming all sources of uncertainty are independent, the validation uncertainty that accounts for all sources of uncertainty is computed using Equation (1) and for the semi-analytical model is estimated to be $\pm 114.3\mu\text{m}$. Thus, the interval within which the modeling error falls for the nominal conditions is $31.3 \pm 114.3\mu\text{m}$. Since the uncertainty of the semi-analytical melt pool model at the given set of parameters is large and beyond the realm of possibility, the percentage variation assumed for absorption coefficient need to be revised. From the DOE analysis and obtained results, the following observations can be made.

- (1) The modeling uncertainty of the semi-analytical-based melt pool model ($E = 31.3\mu\text{m}$ and $u_{val} = 114.3\mu\text{m}$ at nominal parameter setup) is large as expected due to many assumptions and simplifications used regarding heat source, powder layer formation, and melt pool dynamics. Ignoring these phenomena results in larger modeling error,

and thus a model that considers many physical phenomena existing in L-PBF process can have better predictive accuracy.

- (2) The contribution of input parameters uncertainty to the overall modeling uncertainty is more than 100% ($\pm 109.2\%$) for the semi-analytical model. This is mainly due to the large uncertainty value assumed for the input parameters, especially, the absorption coefficient ($\pm 25\%$). The knowledge of parameter uncertainty is necessary for the estimation of modeling uncertainty in which the model accurately determines the response within a specified range of parameters. In addition, the accuracy of the statistically-driven mathematical model can be improved by increasing the number of testing results which requires more simulation runs.
- (3) The contribution of the numerical uncertainty is very small ($\pm 3.4\%$ for semi-analytical) compared to the other sources of uncertainty. This contribution can be considered negligible. The measurement uncertainty used for model validation has a significant contribution to the modeling uncertainty ($\pm 29.9\%$). This large variation can be associated with the calibration of the optical microscope used to capture the image of a scan track, variation of the incandescent light generated by the hot surface (which depends on the temperature and emissivity of the surface), the adjusted exposure time of the camera, and the dynamics of the melt pool, powder, and laser interactions [43].

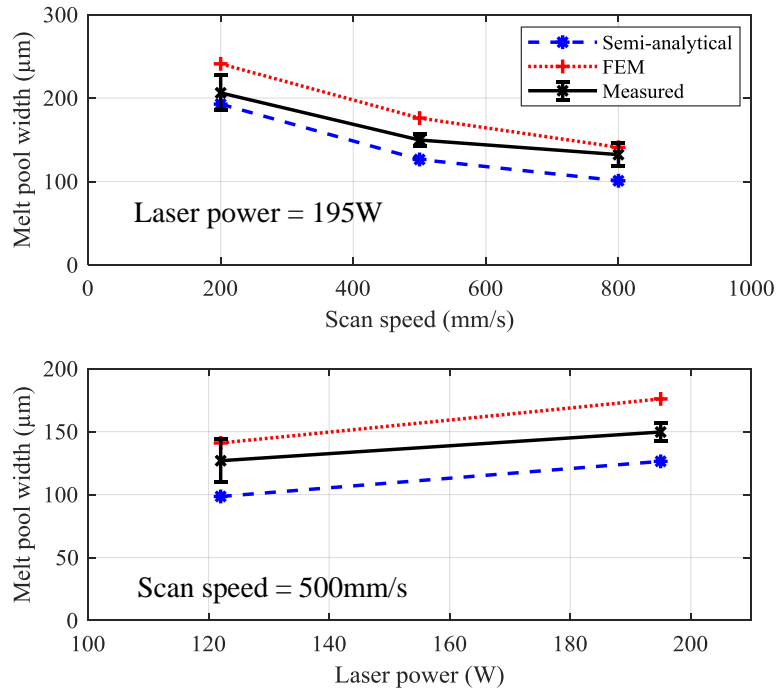


Figure 4: Predicted and measured melt pool width

Conclusions

In this paper, we presented an uncertainty quantification strategy for L-PBF models. A case study was presented with two models: a semi-analytical-based and a FEM melt pool models. A DOE fractional factorial study was conducted with two levels for nine and ten input parameters for the semi-analytical-based and FEM melt pool models, respectively. The DOE models were then used as part of a Monte Carlo simulation to predict melt pool width in order to compute output uncertainty of the models due to uncertainty in input parameters.

The semi-analytical-based melt pool model was computationally efficient to run, but the DOE prediction results had large uncertainty. The FEM melt pool model, though more accurate, posed difficulty when managing uncertainty with the calibration parameters. The DOE study conducted in this paper included only two levels and therefore can only estimate linear effects between the levels. To develop an accurate DOE model for prediction, three or more levels would need to be conducted. This requires an increasingly large number of simulations for quantifying the uncertainty of FEM models.

Future work will involve further refining the amount of uncertainty included in the input parameters and then running the DOE with higher levels that ensure non-linear effects between the levels and among multiple factors. This process will be evaluated for both the semi-analytical-based and FEM-based melt pool models. Refinement of the input uncertainty especially on absorption coefficient and layer thickness is needed as the amount of uncertainty assumed for these parameters is appeared to be too high.

Disclaimer

No approval or endorsement of any commercial product by NIST is intended or implied. Certain commercial equipment, instruments or materials are identified in this report to facilitate better understanding. Such identification does not imply recommendations or endorsement by NIST nor does it imply the materials or equipment identified are necessarily the best available for the purpose.

Acknowledgments

The authors gratefully acknowledge Yan Lu, Brandon Lane, Moneer Helu, William Bernstein, and Thomas Kramer from NIST for their valuable feedback that improved the paper.

References

- [1] Petrovic, V., Vicente Haro Gonzalez, J., Jordá Ferrando, O., Delgado Gordillo, J., Ramón Blasco Puchades, J., and Portolés Griñan, L., 2011, "Additive Layered Manufacturing: Sectors of Industrial Application Shown through Case Studies," *Int. J. Prod. Res.*, 49(4), pp. 1061–1079.
- [2] Wohlers, T., 2016, "Wohlers Report 2016. 3D Printing and Additive Manufacturing State of the Industry," *Wohlers Rep.* 2016, (May), p. 355.
- [3] Coykendall, J., Cotteleer, M., Holdowsky, L., and Mahto, M., 2014, "3D Opportunity in Aerospace

- and Defense,” Deloitte Univ. Press, pp. 1–28.
- [4] Hodge, N. E., Ferencz, R. M., and Vignes, R. M., 2016, “Experimental Comparison of Residual Stresses for a Thermomechanical Model for the Simulation of Selective Laser Melting,” *Addit. Manuf.*, 12, pp. 159–168.
 - [5] Lopez, F., Witherell, P., and Lane, B., 2016, “Identifying Uncertainty in Laser Powder Bed Fusion Additive Manufacturing Models,” *J. Mech. Des.*, 138(November), pp. 1–4.
 - [6] Devesse, W., De Baere, D., and Guillaume, P., 2014, “The Isotherm Migration Method in Spherical Coordinates with a Moving Heat Source,” *Int. J. Heat Mass Transf.*, 75, pp. 726–735.
 - [7] Smith, J., Xiong, W., Cao, J., and Liu, W. K., 2016, “Thermodynamically Consistent Microstructure Prediction of Additively Manufactured Materials,” *Comput. Mech.*, 57(3), pp. 359–370.
 - [8] Schoinochoritis, B., Chantzis, D., and Salonitis, K., 2014, “Simulation of Metallic Powder Bed Additive Manufacturing Processes with the Finite Element Method: A Critical Review,” *Proc. Inst. Mech. Eng. Part B J. Eng. Manuf.*, 231(1), pp. 96–117.
 - [9] Hu, Z., and Mahadevan, S., 2017, “Uncertainty Quantification and Management in Additive Manufacturing: Current Status, Needs, and Opportunities,” *Int. J. Adv. Manuf. Technol.*, pp. 1–20.
 - [10] Zhou, J., Zhang, Y., and Chen, J. K., 2009, “Numerical Simulation of Random Packing of Spherical Particles for Powder-Based Additive Manufacturing,” *J. Manuf. Sci. Eng.*, 131(3), pp. 1–8.
 - [11] Herbold, E. B., Walton, O., and Homel, M. A., 2015, “Simulation of Powder Layer Deposition in Additive Manufacturing Processes Using the Discrete Element Method,” LLNL-TR-678550.
 - [12] Boley, C. D., Khairallah, S. A., and Rubenchik, A. M., 2015, “Calculation of Laser Absorption by Metal Powders in Additive Manufacturing,” *Appl. Opt.*, 54(9), pp. 2477–82.
 - [13] Gusarov, A. V., and Kruth, J. P., 2005, “Modelling of Radiation Transfer in Metallic Powders at Laser Treatment,” *Int. J. Heat Mass Transf.*, 48(16), pp. 3423–3434.
 - [14] Bo Cheng; Kevin Chou, 2015, “Melt Pool Evolution Study in Selective Laser Melting,” *Dyn. Syst. with Appl. using MATLAB*, 53(August), pp. 1182–1194.
 - [15] Khairallah, S. A., Anderson, A. T., Rubenchik, A., and King, W. E., 2016, “Laser Powder-Bed Fusion Additive Manufacturing: Physics of Complex Melt Flow and Formation Mechanisms of Pores, Spatter, and Denudation Zones,” *Acta Mater.*, 108, pp. 36–45.
 - [16] Li, X., and Tan, W., 2017, “3-Dimensional Cellular Automata Simulation of Grain Structure in Metal Additive Manufacturing Processes,” *Solid Free. Fabr. 2017 Proc. 28th Annu. Int. Solid Free. Fabr. Symp. – An Addit. Manuf. Conf.*, pp. 1030–1047.
 - [17] Keller, T., Lindwall, G., Ghosh, S., Ma, L., Lane, B. M., Zhang, F., Kattner, U. R., Lass, E. A., Heigel, J. C., Idell, Y., Williams, M. E., Allen, A. J., Guyer, J. E., and Levine, L. E., 2017, “Application of Finite Element, Phase-Field, and CALPHAD-Based Methods to Additive Manufacturing of Ni-Based Superalloys,” *Acta Mater.*, 139, pp. 244–253.
 - [18] Zaeh, M. F., and Branner, G., 2010, “Investigations on Residual Stresses and Deformations in Selective Laser Melting,” *Prod. Eng.*, 4(1), pp. 35–45.
 - [19] Cheng, B., Shrestha, S., and Chou, K., 2016, “Stress and Deformation Evaluations of Scanning Strategy Effect in Selective Laser Melting,” *Addit. Manuf.*, 12, pp. 240–251.
 - [20] Lopez, F., Witherell, P., and Lane, B., 2016, “Identifying Uncertainty in Laser Powder Bed Fusion Additive Manufacturing Models,” *Proc. ASME 2016 Int. Manuf. Sci. Eng. Conf. MSEC2016 June 27-July 1, 2016, Blacksburg, Virginia, USA*, 138(November), pp. 1–10.
 - [21] Assouroko, Ibrahim; Lopez, Felipe; Witherell, P., 2016, “A Method for Characterizing Model Fidelity in Laser Powder Bed Fusion Additive Manufacturing,” *Proc. ASME 2016 Int. Mech. Eng. Congr. Expo. ASME IMECE 2016 Novemb. 11-17, 2016, Phoenix, Arizona, USA*, pp. 1–13.
 - [22] Tapia, G., and Elwany, A., 2014, “A Review on Process Monitoring and Control in Metal-Based Additive Manufacturing,” *J. Manuf. Sci. Eng.*, 136(6), pp. 060801-1-060801-10.
 - [23] Garg, A., Tai, K., and Savalani, M. M., 2014, “State-of-the-Art in Empirical Modelling of Rapid Prototyping Processes,” *Rapid Prototyp. J.*, 20(2), pp. 164–178.
 - [24] Partee, B., Hollister, S. J., and Das, S., 2006, “Selective Laser Sintering Process Optimization for Layered Manufacturing of CAPA 6501 Polycaprolactone Bone Tissue Engineering Scaffolds,” *J.*

- Manuf. Sci. Eng., 128(2), pp. 531–540.
- [25] Adamczak, S., Bochnia, J., and Kaczmarek, B., 2014, “Estimating the Uncertainty of Tensile Strength Measurement for a Photocured Material Produced by Additive Manufacturing,” *Metrol. Meas. Syst.*, 21(3), pp. 553–560.
- [26] Delgado, J., Ciurana, J., and Rodríguez, C. A., 2012, “Influence of Process Parameters on Part Quality and Mechanical Properties for DMLS and SLM with Iron-Based Materials,” *Int. J. Adv. Manuf. Technol.*, 60(5–8), pp. 601–610.
- [27] Raghunath, N., and Pandey, P. M., 2007, “Improving Accuracy through Shrinkage Modelling by Using Taguchi Method in Selective Laser Sintering,” *Int. J. Mach. Tools Manuf.*, 47(6), pp. 985–995.
- [28] Kamath, C., 2016, “Data Mining and Statistical Inference in Selective Laser Melting,” *Int. J. Adv. Manuf. Technol.*, 86(5–8), pp. 1659–1677.
- [29] Moser, D., Beaman, J., Fish, S., and Murthy, J., 2014, “Multi-Layer Computational Modeling of Selective Laser Sintering Processes,” *Proc. ASME 2014 Int. Mech. Eng. Congr. Expo. IMECE2014*, pp. 1–11.
- [30] Ma, L., Fong, J., Lane, B., Moylan, S., Filliben, J., Heckert, A., and Levine, L., 2015, “Using Design of Experiments in Finite Element Modeling To Identify Critical Variables for Laser Powder Bed Fusion,” *Solid Free. Fabr. Symp.*, pp. 219–228.
- [31] Nath, P., Hu, Z., and Mahadevan, S., 2017, “Multi-Level Uncertainty Quantification in Additive Manufacturing,” *Solid Free. Fabr. 2017 Proc. 28th Annu. Int. S.*, pp. 922–937.
- [32] King, W. E., Anderson, A. T., Ferencz, R. M., Hodge, N. E., Kamath, C., Khairallah, S. A., and Rubenchik, A. M., 2015, “Laser Powder Bed Fusion Additive Manufacturing of Metals; Physics, Computational, and Materials Challenges,” *Appl. Phys. Rev.*, 2(4), p. 041304.
- [33] ASME-V&V-20, 2009, *An Overview of ASME V&V 20: Standard for Verification and Validation in Computational Fluid Dynamics and Heat Transfer*, American Society of Mechanical Engineers.
- [34] Schwer, L. E., 2008, “Is Your Mesh Refined Enough? Estimating Discretization Error Using GCI,” *7th LS-DYNA Anwenderforum*, 1(1), pp. 45–54.
- [35] Roache, P., 2002, “Code Verification by the Method of Manufactured Solutions,” *ASME J. Fluids Engineer.*, 114(1), pp. 4–10.
- [36] Montgomery, D. C., 2012, *Design and Analysis of Experiments*, John Wiley & Sons, Inc.
- [37] Mahesh, M., Lane, B., Donmez, A., Feng, S., Moylan, S., and Fesperman, R., 2015, “Measurement Science Needs for Real-Time Control of Additive Manufacturing Powder Bed Fusion Processes,” *Natl. Inst. Stand. Technol.*, pp. 1–50.
- [38] Slotwinski, J. A., Garboczi, E. J., Stutzman, P. E., Ferraris, C. F., Watson, S. S., and Peltz, M. A., 2014, “Characterization of Metal Powders Used for Additive Manufacturing,” *J. Res. Natl. Inst. Stand. Technol.*, 119, pp. 460–493.
- [39] Cooke, A., and Slotwinski, J., 2015, “Properties of Metal Powders for Additive Manufacturing: A Review of the State of the Art of Metal Powder Property Testing,” *Addit. Manuf. Mater. Stand. Test. Appl.*, pp. 21–48.
- [40] JCGM, 2008, “Evaluation of Measurement Data — Guide to the Expression of Uncertainty in Measurement,” *Int. Organ. Stand. Geneva ISBN*, 50(September), p. 134.
- [41] Hassanpour, R. M., 2010, “Application of Experimental Design in Uncertainty Quantification,” *Pap. CCG Annu. Rep.*, 126(12), pp. 1–6.
- [42] NIST/SEMATECH e-Handbook of Statistical Methods, <http://www.itl.nist.gov/div898/handbook/>, [last accessed: August 31, 2018].
- [43] Fox, J. C., Lane, B. M., and Yeung, H., 2017, “Measurement of Process Dynamics through Coaxially Aligned High Speed Near-Infrared Imaging in Laser Powder Bed Fusion Additive Manufacturing,” *Proc. SPIE 10214, Thermosense: Thermal Infrared Applications XXXIX 1(301)*, pp. 1021407